

Article

Ultraviolet Exposure Improves SERS Activity of Graphene-Coated Ag/ZrO₂ Substrates

Hanna Bandarenka ¹, Aliaksandr Burko ¹, Diana Laputsko ¹, Lizaveta Dronina ¹, Nikolai Kovalchuk ¹, Alise Podelinska ^{2,3}, Uladzislau Shapel ², Anatoli I. Popov ² and Dmitry Bocharov ^{2,*}

¹ Micro- and Nanoelectronics Department, Belarusian State University of Informatics and Radioelectronics, 220013 Minsk, Belarus; h.bandarenka@bsuir.by (H.B.); a.burko@bsuir.by (A.B.); d.laputko@bsuir.by (D.L.); e.dronina@bsuir.by (L.D.); n.kovalchuk@bsuir.by (N.K.)

² Institute of Solid State Physics, University of Latvia, LV-1063 Riga, Latvia; alisep@cfi.lu.lv (A.P.); uladzislau.shapel@cfi.lu.lv (U.S.); popov@latnet.lv (A.I.P.)

³ Institute of Physics, University of Tartu, 50411 Tartu, Estonia

* Correspondence: bocharov@cfi.lu.lv

Abstract: This study reveals a significant improvement in surface-enhanced Raman scattering (SERS) activity of Ag/ZrO₂ substrates covered with a few-layer graphene preliminary exposed to ultraviolet (UV) light. The SERS-active substrates are formed by the “silver mirror” deposition of Ag nanoparticles on annealed zirconia blocks. The film composed of ~3 graphene layers is grown on copper foil by a chemical vapor deposition and then wet-transferred to the SERS-active substrates. The graphene-free Ag/ZrO₂ samples are found to provide an enhancement of the Raman scattering from rhodamine 6G (R6G) at a micromolar concentration, which is associated with combined effects from the surface plasmon resonance in the Ag nanoparticles and a charge transfer facilitated by zirconium dioxide. It is revealed that the SERS signal from the analyte molecules can be suppressed by a UV exposure of the Ag/ZrO₂ samples due to photocatalytic activity of the wide band gap semiconductor. However, if the samples are covered with a few-layer graphene (Gr/Ag/ZrO₂) it prevents the dye molecule decomposition upon the UV treatment and improves SERS activity of the substrates. The 365 nm treatment leads to a 40% increase in the 10⁻⁶ M R6G SERS spectrum intensity, while the 254 nm irradiation causes it to rise by 47%, which is explained by different responses from the surface and bulk zirconia crystals to the short and long UV wavelengths. This enhancement is attributed to the distinct responses of surface and in-depth zirconia crystals to varied UV wavelengths and underscores the pivotal role of graphene as a protective and enhancing layer.

Keywords: a few-layer graphene; wide bandgap semiconductor; zirconia dioxide; silver nanoparticles; surface-enhanced Raman scattering; photocatalytic activity; charge transfer



Citation: Bandarenka, H.; Burko, A.; Laputsko, D.; Dronina, L.; Kovalchuk, N.; Podelinska, A.; Shapel, U.; Popov, A.I.; Bocharov, D. Ultraviolet Exposure Improves SERS Activity of Graphene-Coated Ag/ZrO₂ Substrates. *Crystals* **2023**, *13*, 1570. <https://doi.org/10.3390/cryst13111570>

Academic Editors: Justina Gaidukevic and Jurgis Barkauskas

Received: 7 October 2023

Revised: 25 October 2023

Accepted: 31 October 2023

Published: 3 November 2023



Copyright: © 2023 by the authors. Licensee MDPI, Basel, Switzerland. This article is an open access article distributed under the terms and conditions of the Creative Commons Attribution (CC BY) license (<https://creativecommons.org/licenses/by/4.0/>).

1. Introduction

In recent years, a trend towards the use of graphene-containing nanomaterials as tools for the surface enhancement of Raman scattering (SERS) has become strongly pronounced [1,2]. In general, a graphene story in SERS spectroscopy began a little over a decade ago from a formation of gold nanoparticles and dendrites on graphene oxide nanosheets [3,4]. Graphene has been found to quench fluorescence from analyte molecules [5] and to enhance Raman scattering via chemical mechanism [6]. In [7] the SERS-active substrate based on the paper strip modified with graphene and Ag nanoparticles was shown to facilitate detection of rhodamine 6G at 10⁻¹⁹ M concentration. A bit later, the few-layer graphene was found to be an efficient protective layer to prevent burning analyte molecules during SERS analysis, which provided the detection of lactoferrin protein adsorbed on the SERS-active surface from the 10⁻¹⁸ M solution [8]. Therefore, graphene has been proved to possess multifunctional properties that are extremely fruitful for SERS

spectroscopy in terms of decreasing electromagnetic field influence on analyte molecules leading to the side effects in the SERS spectra [9,10].

Wide band gap (WBG) semiconductors are other rather “fresh” materials that can potentially lead to engineering the SERS-active substrates possessing athermal and self-cleaning properties [11–14]. The first feature allows SERS measurements to be free of the thermal-induced destruction of analyte molecules, thus improving analysis reliability [11]. At the same time, the UV-facilitated cleaning of the SERS-active substrates which have passed through the analysis cycle is of high demand in affordability terms [14]. Considering that SERS-active substrates are consumable tools of SERS spectroscopy, they should be cost-effective or reusable for wide implementation of such analytical techniques in clinical practice, forensic science, and pharmaceuticals, to name a few.

Taking the above into account, the question arises: what kind of breakthroughs could the combination of graphene, plasmonic nanostructures, and WBG semiconductors bring to ultrasensitive molecular analysis by SERS spectroscopy? Very recently, gold-coated TiO₂ microparticles wrapped with reduced graphene oxide piqued the interest of researchers owing to their capability of amplifying SERS activity and providing photocatalytic degradation of organic pollutants [15]. In such cases, the Raman signal enhancement is attributed to a plethora of mechanisms inherent in these heterostructures. The presence of noble metal nanostructure in the substrate bolsters the electromagnetic field at the surface—a phenomenon attributed to its surface plasmonic resonance [16]. This enhancement in the electromagnetic field is instrumental in amplifying the Raman signal of molecules adsorbed on the surface. Graphene, characterized by its extraordinary electrical conductivity, augments the SERS effect. In conjunction with noble metal, graphene facilitates an increase in the charge transfer, contributing further to the electromagnetic field at the surface [17]. This synergy between graphene and metal emerges as a pivotal factor in the SERS activity improvement [18]. Moreover, graphene’s pronounced absorption of UV light enriches the light–matter interaction at the hosting WBG semiconductor surface, offering the avenue for its prominent photocatalytic activity for the destruction of organic molecules after their detection [15]. The multifaceted role of graphene is not just limited to the charge transfer and UV absorption; it also acts as a heatsink and, thus, slows changing the analyte molecules structure during SERS analysis on the substrate surface [8]. In addition to the synergistic actions of graphene and plasmonic nanostructure, the WBG semiconductor plays a principal role. It avails additional sites for the adsorption of molecules and, in unison with Ag and graphene, is expected to augment Raman signals via charge transfer. However, it is imperative to note that the SERS and photocatalytic effects are contingent upon specific preparations and structure composition of the noble metal/WBG semiconductor and graphene coatings. Variations in these parameters can significantly influence the extent and efficiency of SERS activity upon visible light and photocatalytic features while the UV is irradiating.

Summarizing the above, the combination of graphene, plasmonic structures, and the WBG semiconductor opens new prospects in bringing SERS spectroscopy closer to real practical application. The goal of this work was to reveal the applicability of the sandwich structure based on a few-layer graphene, silver particles, and zirconia substrates for design and engineering the nanomaterial combining expressed SERS activity and photocatalytic properties. The silver was selected since it bears the most powerful surface plasmon efficiency among other metals [19]. Zirconia was used as a host semiconductor for the plasmonic nanomaterial because it is often characterized by band gap over 5 eV [20]. This is good for the photocatalytic activity at the far-UV light, which, in turn, can provide the most effectual destructive effect on the molecules to clean the SERS-active substrate from them after analysis. Furthermore, modification of ZrO₂-based structures with silver have already been reported elsewhere as a powerful approach to improve the zirconia surface reactivity for electrochemical determination of tinidazole antibiotic [21], photo electro chemical degradation of methylene blue [22,23], and quantitative SERS detection of hexavalent chromium in the wastewater [24].

2. Materials and Methods

2.1. Materials

The Cercon ht 98-mm disk, manufactured by Dentsply International Inc., York, PA, USA, was used to prepare ZrO₂-based substrates. Rhodamine 6G (R6G), AgNO₃ (ACS reagent, ≥99.0%), NaOH (reagent grade, 97%), NH₃ (anhydrous, ≥99.98%), and C₄H₄KNaO₆·4H₂O (ACS reagent, ≥99.0%) were supplied by Sigma-Aldrich and used without additional purification. For the transfer of silver films from the ZrO₂ substrates, a poly mer support constructed from SU-8 2015 was used, sourced from MicroChem, Newton, MA, USA. Water was purified with Milli-Q system (Millipore, Bedford, MA, USA).

2.2. Fabrication of SERS-Active Substrates

The Cercon disk was meticulously cut into blocks measuring 8 × 6 × 14 mm, serving as the ZrO₂-based substrates. The blocks were annealed in air following the temperature regimes displayed in Table 1, which led to their approx. 20% shrinking. Then we formed a plasmonic coating composed of silver nanoparticles on the ZrO₂ blocks. Prior to this, each block was treated with a piranha solution, consisting of H₂SO₄:H₂O₂ at a 3:1 volume ratio, and maintained at a temperature between 70–80 °C for 5 min to slightly roughen its surface for further improvement of metal coating adhesive strength. Ag nanoparticles were grown by the “silver mirror” method in a mixture of basic solution (4 mL), reducing solution (1 mL), and ethanol (1 mL) [11,25]. Basic and reducing solutions were water solutions of 0.07 M AgNO₃, 0.2 M NaOH, 0.6 M NH₃, and 0.4 M C₄H₄KNaO₆·4H₂O, respectively. The ZrO₂ blocks were immersed in the “silver mirroring” solution for 6 min. After the silver deposition, the samples were rinsed with deionized water and air-dried at 21 °C temperature.

Table 1. Regimes of the ZrO₂ block annealing.

Step	Starting Temperature, °C	Final Temperature, °C	Time, min	Rate, °C/min
1	50	−2	0	−
2	50	300	40	7.5
3	300	800	100	5.0
4	800	1300	200	2.5
5	1300	1530	46	5.0
6	1500	1530	120	Keeping 1530 °C
7	1530	20	−	Cooling

2.3. Few-Layer Graphene Formation and Transfer

The synthesis of few-layer graphene (Gr) was performed by chemical vapor deposition (CVD) from methane, a method thoroughly detailed in reference [8]. In this process, copper foil samples, electrochemically polished to perfection, were initially annealed at a temperature of 1050 °C for 1 h. This was conducted under the constant purge flows of argon and hydrogen, delivered at flow rates of 100 and 150 cm³/min, respectively. Then, the H₂ flow rate was reduced to 15 cm³/min and methane was bled in at the flow rate of 1.3 cm³/min for 30 min. After the synthesis, the surface of the Cu foil facing the walls of the quartz reactor was worked up in an oxygen plasma to remove so-called unwanted graphene. The grown few-layer graphene was transferred to the ZrO₂-based blocks using a wet chemical technique. Firstly, the samples were immersed an aqueous solution of FeCl₃ until complete copper dissolution while the graphene film remained floating on the solution’s surface. Before the graphene transfer, this solution was three times totally replaced with deionized water by pipette suction and filling. This step was introduced to minimize undesirable adsorption of the side reaction products on the surface of the SERS-active substrates. The transferring procedure was conducted by the ZrO₂-based blocks’ immersion in the solution under the graphene film and its lifting up. As a result, the graphene film remained on the surface of the substrate.

2.4. Characterization of the Experimental Samples

The ZrO₂ and Ag/ZrO₂ substrates underwent a thorough structural characterization, facilitated by the advanced Hitachi S-4800 (Hitachi Limited, Tokyo, Japan) scanning electron microscope (SEM) stationed in Tokyo, Japan. Elemental composition of the same samples was defined with a Bruker QUANTAX 200 (Bruker Nano GmbH, Adlershof, Berlin, Germany) energy dispersive X-ray (EDX) spectrometer embedded onto the scanning electron microscope. This equipment provided the elemental distribution and composition, ensuring an exhaustive characterization.

Raman and SERS analysis was performed with a 3D confocal Raman microscope–spectrometer Confotec NR500 (SOL Instruments, Minsk, Belarus). The measurements were taken using 473 or 633 nm laser and a 100× objective (NA = 0.95). The power of both laser beams passed through the objective was 4.66 ± 0.005 mW.

The spectra of the few-layer graphene were collected using the 633 nm laser. The few-layer graphene was transferred to the cover glass and Ag/ZrO₂ sample for the Raman and SERS measurements to find out if the SERS activity affects the graphene structure.

The reproducibility of the SERS signal provided by the Ag/ZrO₂ and Gr/Ag/ZrO₂ substrates was studied with a testing analyte presented by rhodamine 6G (R6G) molecules dissolved in deionized water. Prior to the SERS measurements, the substrates were kept in the 10^{−6} M analyte solution for 2 h, rinsed with deionized water for 30 s to remove an excess of unabsorbed molecules, and air-dried. The arrays of spectra (100 in total) were collected by scanning the 100 × 100 μm spot on the SERS-active surface with a focused 473 nm laser beam.

2.5. Study of Photocatalytic Activity

Photocatalytic activity of the zirconia-based samples was assessed by comparing specific band intensity in the R6G SERS spectra before and after the UV exposure. Firstly, the dye molecules were deposited on the Ag/ZrO₂ and Gr/Ag/ZrO₂ samples from 10^{−6} M R6G solutions followed by collecting their SERS spectra. Then, each substrate was immersed in a Petri dish of 3 cm diameter filled with 3 mL of deionized water and subjected to the UV irradiation for different times. Parallel with this process, control samples, utilizing commercial SERS-active substrates referenced in [26], underwent identical UV treatment procedures to offer a comparative analysis of the photocatalytic activity. Testing the photocatalytic activity in a Petri dish filled with water was based on the rationale that it facilitates the desorption of decomposed dye molecules from the substrate surface into the liquid medium, resulting in an improved cleaning compared to cleaning solely in water under UV-free conditions. The UV exposure was provided by a VL-6. LC Vilber appliance (Vilber, Collegen, France) equipped with 254 and 365 nm wavelength lamps. This equipment ensured uniform and precise UV irradiation, which is essential for an accurate assessment of photocatalytic activity. After that, all the samples were rinsed with deionized water for 30 s, air-dried, and the SERS measurements were repeated.

3. Results and Discussion

3.1. Structure of the Experimental Samples

3.1.1. ZrO₂ and Ag/ZrO₂ Substrates

The ZrO₂ block surface is characterized by grainy morphology, as seen in Figure 1a. The grains, displaying a size variation from 225 nm to approximately 1.5 μm, predominantly fall within the 400–600 nm range. The black curve in the Raman spectrum of Figure 1b reveals the polycrystalline nature of the zirconia block (ZrO₂—1), evidenced by the distinct bands representative of tetragonal (~243, ~298, ~458, and ~631 cm^{−1}) and monoclinic (~200 and ~374 cm^{−1}) lattices [27,28]. The band at 458 cm^{−1} can be attributed to tetragonal zirconia stabilized with yttrium oxide [29], of which a small amount is present in the Cercon disk.

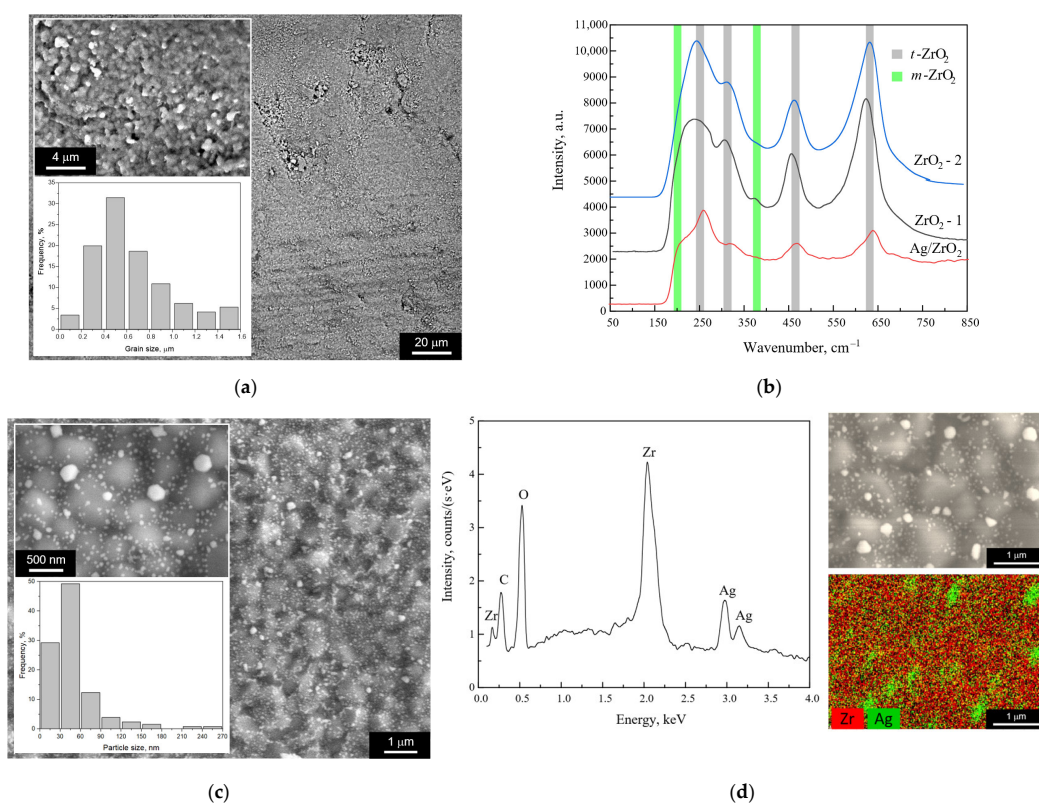
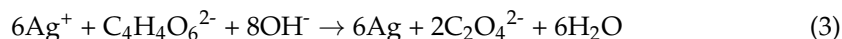
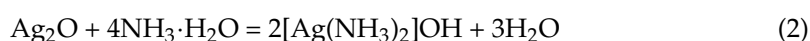
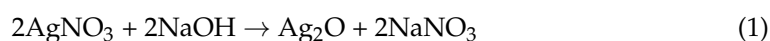


Figure 1. Structural characterization of the samples: (a) SEM top view images of the ZrO₂ substrate and the ZrO₂ grain size distribution histogram; (b) Raman spectra of the ZrO₂—1, Ag/ZrO₂, and ZrO₂—2 substrates; (c) SEM top view images of the Ag/ZrO₂ substrate and the Ag particle size distribution histogram; (d) EDX spectrum and EDX scan of the Ag/ZrO₂ substrate.

To infuse SERS activity into the zirconia substrate, it was submerged in the “silver mirror” solution, resulting in a uniform deposition of silver. This process is detailed through the following chemical reactions:



The “silver mirror” chemical method was selected due to the WBG nature of zirconia [30,31]; other wet techniques, like corrosive and electrochemical deposition, are hardly applicable to growing silver particles on the ZrO₂ surface. Figure 1c depicts the SEM top view images of the zirconia block subjected to the silver deposition. The silver coating is constituted by nanoparticles, the majority of which have sizes of nanoscale range between a few nanometers and 90 nm. However, a small fraction, approximately 10%, of the Ag nanostructures, is characterized by larger sizes up to 270 nm as seen from the histogram in Figure 1c. The post-“silver mirroring” Raman spectrum of the zirconia block, depicted by the red curve in Figure 1b, is characterized by the suppressed Raman bands of ZrO₂ as a direct consequence of the silver coating. The silver deposition led to suppressing the 374 cm^{−1} band (responsible for the m-lattice) down to negligible intensity. This allows for the suggestion of the partial phase transformation of zirconia upon the Ag deposition. At the same time, the band at approx. 200 cm^{−1} appears more prominent after the silver deposition, which gives rise to controversial opinion. That is why we additionally studied

Raman spectrum of the zirconia sample subjected to removal of Ag coating with hydrochloric acid. This sample is marked as $\text{ZrO}_2\text{---}2$ in Figure 1b. Indeed, the new spectrum proves the Ag deposition can lead to the phase transformation since no band at approx. 375 cm^{-1} is observed and, also, the band at approx. 200 cm^{-1} looks more hidden by the $t\text{-ZrO}_2$ band at 250 cm^{-1} . This effect is explained by the surface zirconia lattice aligning to the Ag cubic lattice. Slight restructuring the zirconia surface is expected to improve an adhesion of the silver coating and provide faster charge transfer from the WBG substrate via the silver nanoparticles to the analyte molecules during the SERS measurements.

We also should note that no bands of Ag_2S typical for the Raman spectra of nanostructured silver [32,33] are observed. This means there is a rather good chemical stability of the Ag nanoparticles when taking electrons by (or oxidation with) sulfur ions from the environment, which is typical for silver surfaces [34]. The EDX spectrum and EDX scan in Figure 1d prove the Ag nanoparticles presence and uniform distribution on the sample surface.

3.1.2. Few-Layer Graphene

To study the Gr structure in more detail, it was characterized by Raman spectroscopy. As a rule, the graphene Raman spectrum contains G, 2D, and D prominent bands [35,36]. The first one ($\sim 1582\text{ cm}^{-1}$) is attributed to a doubly degenerated phonon mode of E_{2g} symmetry from the center of the Brillouin zone. The 2D band ($\sim 2710\text{ cm}^{-1}$) appears as a result of the resonant light scattering in which two equal-energy phonons are involved. However, the light is scattered in the opposite direction of the pulse, thus providing data on the graphene layers order. The last band ($\sim 1352\text{ cm}^{-1}$) helps to reveal defects in the graphene layers. Therefore, the Raman mapping of graphene on copper was performed. A laser with excitation energy 2.62 eV ($\lambda = 473\text{ nm}$) was utilized. The size of the mapped area was $48 \times 48\ \mu\text{m}^2$. The number of points on the map was 20×20 . The intensities, positions, and half-widths of the Raman spectral bands were determined using the Lorentz approximation. The correlation between the position of the 2D band and the position of the G band was plotted based on data from Raman mapping (Figure 2). The correlation analysis of the G and 2D bands positions was based on that developed in the [37,38] approach, indicating a few-layer structure of graphene (~ 3 layers), which was confirmed using transmission optical spectroscopy (Figure 3).

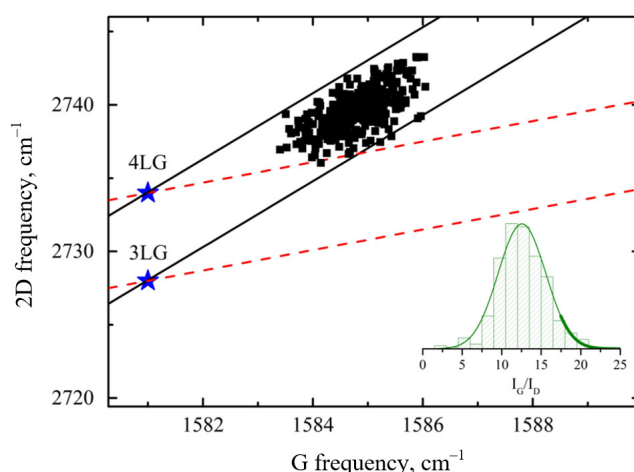


Figure 2. Experimental dependences of 2D band position on position of G band for graphene on copper. The bold solid line (with a slope of ~ 2.2) passing through the blue star marks are responsible for the biaxial strain in the ideal graphene. Dashed red lines (with a slope of ~ 0.7) are responsible for the charge carrier concentration with fixed biaxial strain. The blue star markers correspond to unstressed and undoped multilayer graphene [38] defined taking into account the excitation wavelength used in current work [39] Inset: histogram of the ratio of the intensities of the G band to the D band.

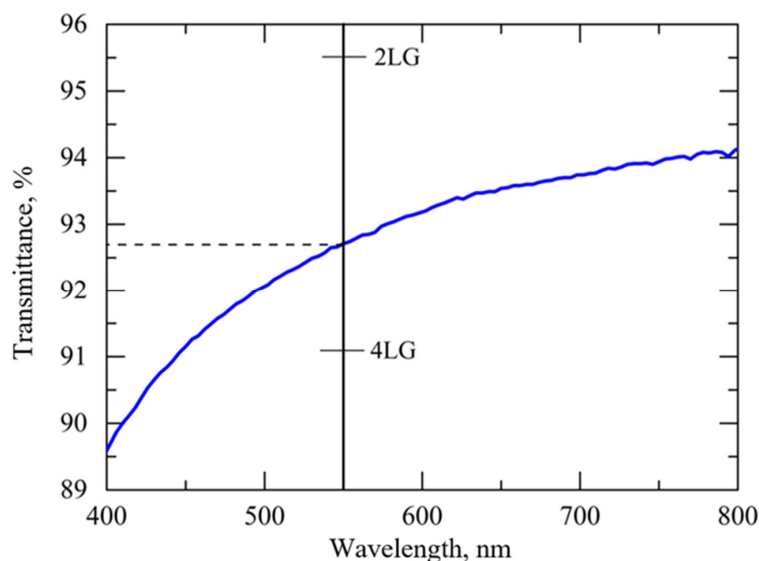


Figure 3. Transmission spectrum of graphene transferred onto the quartz glass.

The intensities, position of the G and 2D bands, and their full width at half-maximum were indicative of a few-layer structure of graphene (~3 layers), which was confirmed using transmission optical spectroscopy (Figure 3).

The transmittance at 550 nm is ~92.7%, which perfectly agrees with transmittance for 3 layered graphene (92.66%) calculated using the following formula [40]:

$$T = (1 + 1.13\pi\alpha N/2)^{-2}, \quad (4)$$

where N is the number of layers and α is the fine-structure constant [41].

The D $\sim 1352\text{ cm}^{-1}$ band, which is responsible for deformation, disorder, and defects in the crystalline structure of graphene, has low intensity compared to the G band (inset Figure 2), so this proves the good quality of the graphene [35].

Subsequently, the few-layer graphene films formed by the CVD method were transferred from the copper foil onto the Ag/ZrO₂ substrates before further studying their structural properties. Figure 4 shows the SEM image of the silver-coated zirconium oxide surface after the Gr film transfer. It can be clearly seen that the surface of the Ag/ZrO₂ substrate has a coating with a small number of folds and holes, which should be a film containing graphene. This was also confirmed by the Raman spectroscopy analysis (Figure 5).

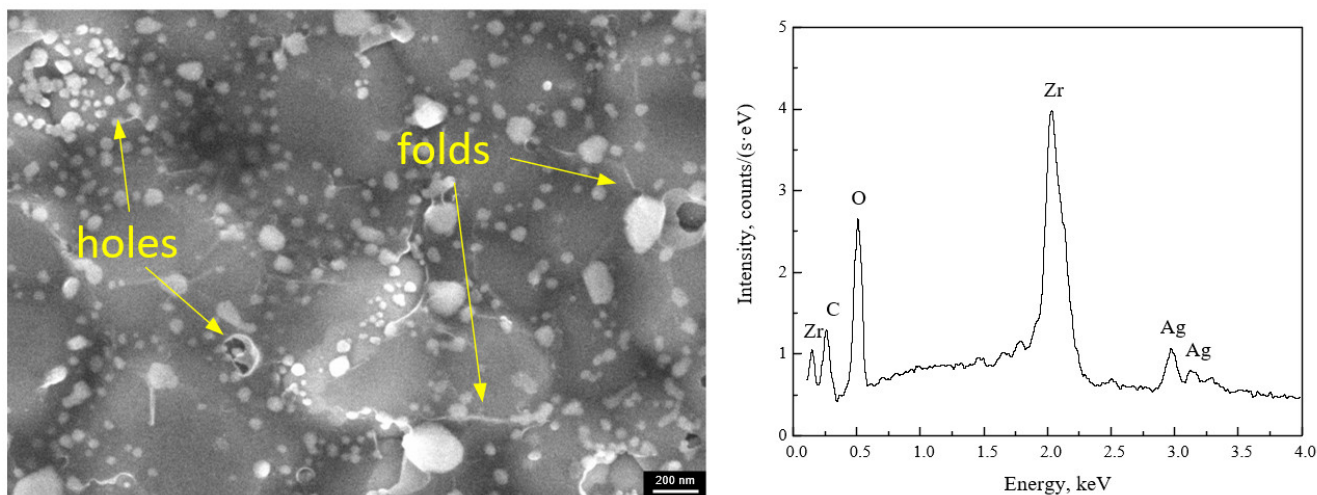


Figure 4. SEM top view image and EDX spectrum of the Gr/Ag/ZrO₂ sample.

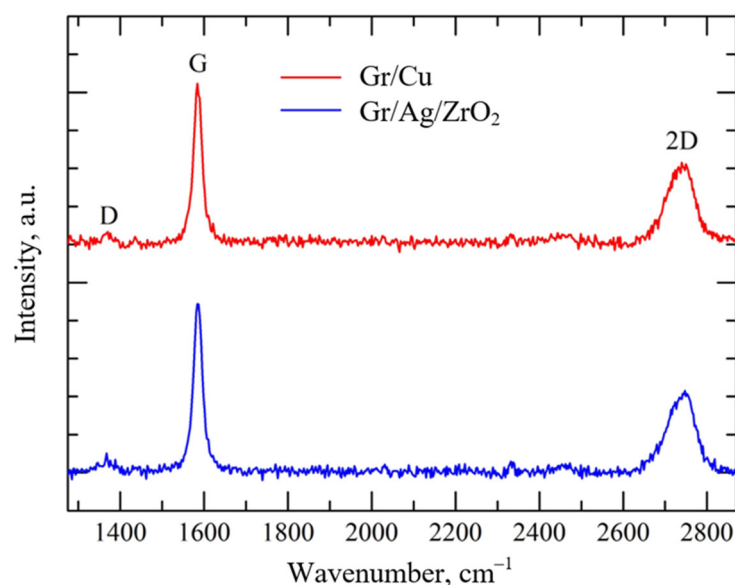


Figure 5. Typical Raman spectrum of graphene on copper and transferred onto an Ag/ZrO₂.

3.2. SERS Activity of the Experimental Samples

Before commencing the SERS measurements, the Ag/ZrO₂ and Gr/Ag/ZrO₂ substrates were immersed in 10⁻⁶ M R6G solution for 2 h for the analyte molecules adsorption. Then, the substrates were rinsed thoroughly with deionized water for 30 s for the removal of the unabsorbed molecules, before being dried. Such procedure was used to provide coating to the substrates with a monomolecular layer of the analyte molecules.

Both the substrates demonstrated SERS activity as seen in Figure 6a since all characteristic R6G Raman bands can be clearly distinguished in the SERS spectra [42,43]. Interestingly, the few-layer graphene provided a triple increase in the SERS spectrum intensity compared to that collected on the Gr-free substrates.

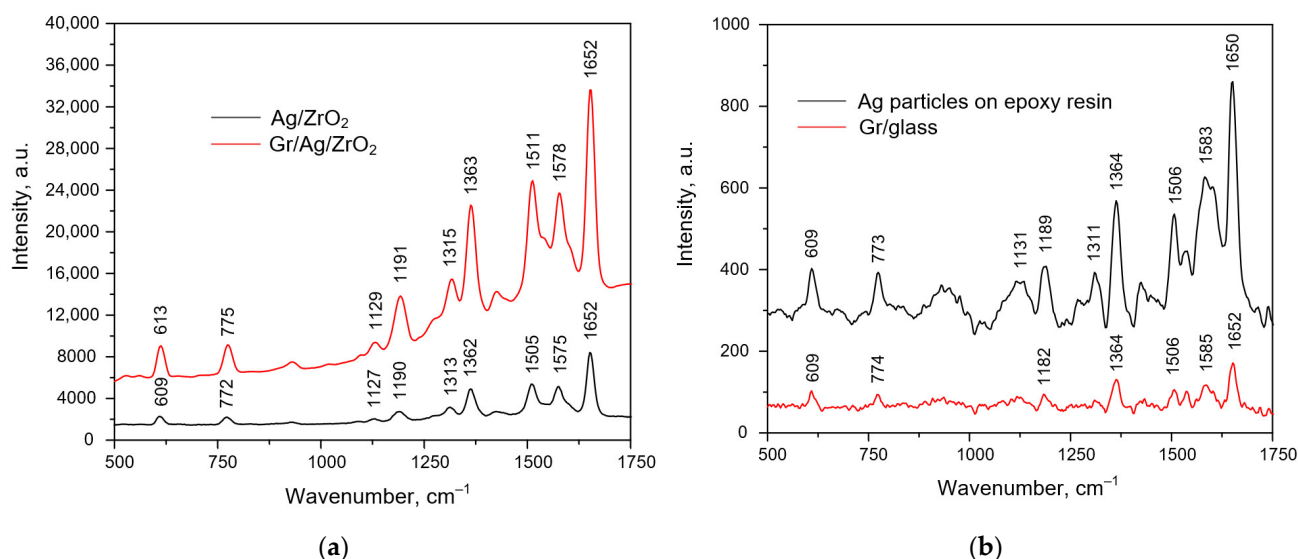


Figure 6. Mean SERS spectra of R6G molecules adsorbed from 10⁻⁶ M solution on the surface of the different substrates: (a) Ag/ZrO₂ and Gr/Ag/ZrO₂; and (b) Ag particles on epoxy resin and Gr/glass.

To further investigate the SERS activity intrinsic to the few-layer graphene, R6G molecules were adsorbed onto the Gr/glass sample. As seen in Figure 6b, the Gr film

facilitates the weak enhancement of the analyte Raman spectrum, which is over two orders of magnitude lower compared with the SERS spectrum collected with the Gr/Ag/ZrO₂ substrate. Also, we tried to evaluate the contribution of the Ag nanoparticles to the Raman spectrum enhancement. The Ag layer was detached from the ZrO₂ block with the epoxy resin film, which was then coated with R6G molecules and studied using the Raman spectrometer. The black spectrum in Figure 6b proves the SERS activity of the Ag nanoparticles. However, even in combination with the few-layer graphene, it can hardly provide the multiplication of the Raman signal from the analyte molecules up to the SERS spectrum intensity achieved with the Gr/Ag/ZrO₂ substrate.

It should be noted that the ZrO₂ block was not found to enhance Raman signal from the analyte molecules at micromolar concentration. The collection of the Raman signal resulted in background free of characteristic analyte bands. Therefore, we suggest that the prominent SERS activity of the Gr-coated substrate is exclusively caused by the combination of the WBG semiconductor, plasmonic particles, and carbon nanostructure. The grainy ZrO₂ surface acts as a source of a charge transferred to the Gr film. Here, we would like to refer to a few papers that have already proved increasing the charge transfer effect in the defected WBG semiconductors [12]. Considering the submicron sizes of the ZrO₂ grains enriched with developed boundary network between them gives a rise to such an explanation. The defects enhance the charge transfer effect and significantly contribute to the electromagnetic enhancement provided by the silver coating.

3.3. Photocatalytic Activity of the Ag/ZrO₂ Substrates

Zirconia is known as a WBG semiconductor, which possesses photocatalytic activity [44]. In our study, we aimed to ascertain whether the granular ZrO₂ block imparts the self-cleaning property to the SERS-active substrate facilitated by the UV exposure and if the graphene coating enables an improvement of this property. Our findings revealed a discernible decline in the intensity of the SERS spectra of 10⁻⁶ M R6G post-exposure to both 365 and 254 nm lamp irradiation. The longer UV wavelength led to over 2–2.5 times (~40–50%) fewer intensive spectra (Figure 7a).

Noticeable was an increase in the 365 nm exposure time from 30 to 120 min which did not result in better analyte molecules decomposition. In contrast, the 254-nm UV exposure exhibited superior photocatalytic activity on the Ag/ZrO₂ sample, inducing approximately 72% spectral intensity reduction at 30 min and around 86% at 120 min of exposure, as illustrated in Figure 7b. The enhanced efficacy of the shorter wavelength UV light is attributable to its deeper penetration and interaction with the internal zirconia grains, while the near-UV primarily engages the surface layer [27]. The short-wavelength UV is hardly absorbed by zirconia [27] thus interacting just with the surface zirconia structures, while longer UV waves are well-absorbed thanks to the rather wide bandgap [44]. Therefore, 254 nm irradiation would interact with in-depth volume of the zirconia sample, which provides more zirconia crystals compared to the surface layer.

We considered that the UV exposure can cause organic dye decomposition, which can be expressed by the presence of d-metal like silver. To exclude such an effect, we made the SERS measurements with the control commercially available substrates based on the silvered silicon nanostructures [25]. Figure 7c shows the SERS spectra of 10⁻⁶ M R6G collected with such substrates before and after the UV exposure at 365 and 254 nm. Indeed, one can see a negligible decrease in the spectra intensity, which is below 30%. Thus, the R6G decomposition enabled by the ZrO₂-based substrates must be provided by the photocatalytic activity of the WBG semiconductor.

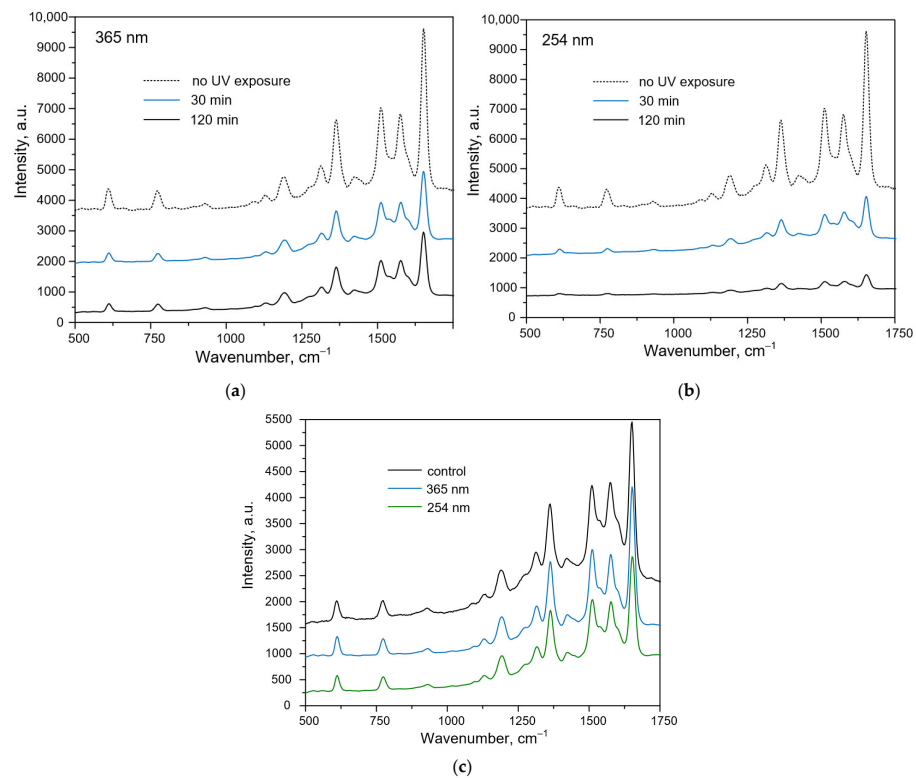


Figure 7. Mean SERS spectra of R6G molecules adsorbed from 10^{-6} M solution on the surface of (a,b) the Ag/ZrO₂ substrates, (c) the control SERS-active substrates, and exposed to 365 nm or 254 nm irradiation.

3.4. Effect of UV Exposure on SERS Activity of the Gr/Ag/ZrO₂ Substrates

The final step of the research was devoted to revealing the UV exposure effect on the Gr/Ag/ZrO₂ substrate properties. The expected improvement of the photocatalytic activity was not found. To the contrary, we observed an undoubted increase in SERS activity because the spectra intensity rose twice (~40%) after the 365 nm exposure and 2.3 time (~47%) in the case of 254 nm irradiation for 2 h (Figure 8), which is explained by the different response of surface and bulk zirconia crystals to the short and long UV wavelengths.

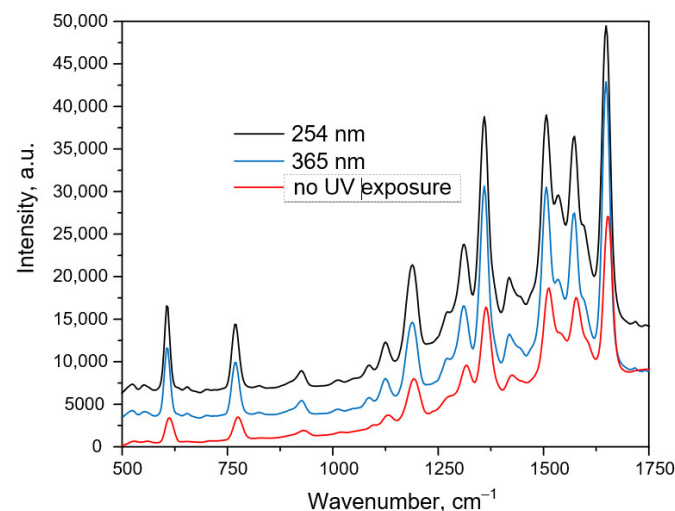


Figure 8. Mean SERS spectra of 10^{-6} M R6G on the Gr/Ag/ZrO₂ substrates before and after the UV exposure.

4. Conclusions

In this study, we investigated the synergistic effects of integrating few-layer graphene, silver particles, and zirconia substrates, unveiling a sophisticated platform for augmented SERS activity and photocatalytic properties.

The SERS-active substrates were formed by the chemical “silver mirror” technique to grow the Ag nanoparticles on the zirconia blocks cured in the furnace. The ZrO₂ surface was found to be composed of the polycrystalline grains with sizes varied from 225 nm to ~1.5 μm. In more detail, the zirconia blocks were shown to have tetragonal and monoclinic lattices as followed from the Raman spectra. The silver nanoparticles were characterized to have sizes of nanoscale range between a few nanometers and 90 nm. The film composed of the ~3 graphene layers was grown on copper foil by the CVD method and then wet-transferred to the SERS-active substrates. Graphene-free Ag/ZrO₂ samples provided the enhancement of the Raman scattering from 10⁻⁶ M R6G, which must be caused by the combined effects from the surface plasmon resonance in the Ag particles and a charge transfer facilitated by zirconium dioxide. However, the SERS signal from the R6G molecules was found to be suppressed by the UV exposure (365 and 254 nm) of the Ag/ZrO₂ samples due to their photocatalytic activity. At the same time, if the Ag/ZrO₂ samples were graphene coated, this prevented R6G decomposition upon the UV treatment and improved SERS activity of the substrates. The 365 nm exposure caused the 40% increase in the 10⁻⁶ M R6G SERS spectrum, while the 254 nm irradiation led to it rising by 47%. Such an effect is under discussion and can be associated with the different responses of surface and bulk zirconia crystals to the short and long UV wavelengths.

In closing, we argue the following key findings:

- Few-layer graphene on Ag-coated zirconia substrates boosts SERS-activity, attributed to enhanced charge transfer from zirconia and silver to analyte molecules via graphene;
- UV exposure, generally, suppresses SERS signals due to zirconia’s photocatalytic activity, but graphene’s integration counters this suppression, emphasizing its role in increasing the SERS signal;
- Our results highlight graphene’s ability to enhance Raman scattering through its versatility in amplifying charge transfer and strengthening electromagnetic interactions.

From the above findings, future directions could involve refining photocatalytic applications by adjusting UV exposure intensity and duration to optimize both self-cleaning capabilities and the analytical performance of SERS-active substrates. Additionally, the synergy between graphene, silver nanoparticles, and zirconia should be further explored to enhance scalability, stability, and adaptability in real-world applications.

In essence, this research underscores a significant stride towards harnessing the combined potential of graphene, silver nanoparticles, and zirconia for advanced SERS applications.

Author Contributions: Conceptualization, H.B. and D.B.; methodology, A.B., L.D., A.P. and N.K.; software, A.B. and U.S.; validation, A.B., D.L., A.P. and H.B.; formal analysis, A.B.; investigation, L.D. and D.L.; resources, H.B., A.I.P. and D.B.; data curation, H.B. and U.S.; writing—original draft preparation, H.B.; writing—review and editing, H.B., A.P., A.I.P. and D.B.; visualization, H.B. and A.B.; supervision, H.B. and D.B.; project administration, H.B. and D.B.; funding acquisition, H.B. and D.B. All authors have read and agreed to the published version of the manuscript.

Funding: This research was funded by the Latvian Scientific Council grant LZP-2021/1-0464 and the State Program for Scientific Research of Belarus “Photonics and Electronics for Innovations” (subprogram “Photonics and its application”, task 1.8; subprogram “Opto- and microwave electronics, task 2.2).

Data Availability Statement: Data are contained within the article.

Acknowledgments: The authors thank Dmitry Karpinsky very much for his kind support during the zirconia block annealing.

Conflicts of Interest: The authors declare no conflict of interest.

References

1. Cao, Y.; Cheng, Y.; Sun, M. Graphene-based SERS for sensor and catalysis. *Appl. Spectrosc. Rev.* **2023**, *58*, 1–38. [CrossRef]
2. Xu, W.; Mao, N.; Zhang, J. Graphene: A Platform for Surface-Enhanced Raman Spectroscopy. *Small* **2013**, *9*, 1206–1224. [CrossRef]
3. Goncalves, G.; Marques, P.A.A.P.; Granadeiro, C.M.; Nogueira, H.I.S.; Singh, M.K.; Grácio, J. Surface Modification of Graphene Nanosheets with Gold Nanoparticles: The Role of Oxygen Moieties at Graphene Surface on Gold Nucleation and Growth. *Chem. Mater.* **2009**, *21*, 4796–4802. [CrossRef]
4. Jasuja, K.; Berry, V. Implantation and Growth of Dendritic Gold Nanostructures on Graphene Derivatives: Electrical Property Tailoring and Raman Enhancement. *ACS Nano* **2009**, *3*, 2358–2366. [CrossRef]
5. Sil, S.; Kuhar, N.; Acharya, S.; Umapathy, S. Is Chemically Synthesized Graphene ‘Really’ a Unique Substrate for SERS and Fluorescence Quenching? *Sci. Rep.* **2013**, *3*, 3336. [CrossRef] [PubMed]
6. Yu, X.; Cai, H.; Zhang, W.; Li, X.; Pan, N.; Luo, Y.; Wang, X.; Hou, J.G. Tuning Chemical Enhancement of SERS by Controlling the Chemical Reduction of Graphene Oxide Nanosheets. *ACS Nano* **2011**, *5*, 952–958. [CrossRef] [PubMed]
7. Yang, C.; Xu, Y.; Wang, M.; Li, T.; Huo, Y.; Yang, C.; Man, B. Multifunctional paper strip based on GO-veiled Ag nanoparticles with highly SERS sensitive and deliverable properties for high-performance molecular detection. *Opt. Express* **2018**, *26*, 10023–10037. [CrossRef] [PubMed]
8. Zavatski, S.; Khinevich, N.; Girel, K.; Redko, S.; Kovalchuk, N.; Komissarov, I.; Lukashevich, V.; Semak, I.; Mamatkulov, K.; Vorobyeva, M.; et al. Surface Enhanced Raman Spectroscopy of Lactoferrin Adsorbed on Silvered Porous Silicon Covered with Graphene. *Biosensors* **2019**, *9*, 34. [CrossRef]
9. Yi, N.; Zhang, C.; Song, Q.; Xiao, S. A hybrid system with highly enhanced graphene SERS for rapid and tag-free tumor cells detection. *Sci. Rep.* **2016**, *6*, 25134. [CrossRef]
10. Jabłońska, A.; Jaworska, A.; Kasztelan, M.; Berbeć, S.; Pałys, B. Graphene and Graphene Oxide Applications for SERS Sensing and Imaging. *Curr. Med. Chem.* **2019**, *26*, 6878–6895. [CrossRef]
11. Girel, K.; Burko, A.; Zavatski, S.; Barysiuk, A.; Litvinova, K.; Eganova, E.; Tarasov, A.; Novikov, D.; Dubkov, S.; Bandarenka, H. Atomic layer deposition of hafnium oxide on porous silicon to form a template for athermal SERS-active substrates. *Appl. Phys. A* **2023**, *129*, 294. [CrossRef]
12. Song, G.; Cong, S.; Zhao, Z. Defect engineering in semiconductor-based SERS. *Chem. Sci.* **2022**, *13*, 1210–1224. [CrossRef]
13. He, R.; Lai, H.; Wang, S.; Chen, T.; Xie, F.; Chen, Q.; Liu, P.; Chen, J.; Xie, W. Few-layered vdW MoO₃ for sensitive, uniform and stable SERS applications. *Appl. Surf. Sci.* **2020**, *507*, 145116. [CrossRef]
14. Zhao, X.; Wang, W.; Liang, Y.; Fu, J.; Zhu, M.; Shi, H.; Lei, S.; Tao, C. Visible-light-driven charge transfer to significantly improve surface-enhanced Raman scattering (SERS) activity of self-cleaning TiO₂/Au nanowire arrays as highly sensitive and recyclable SERS sensor. *Sens. Actuators B Chem.* **2019**, *279*, 313–319. [CrossRef]
15. Zhao, B.; Liu, H.; Xia, L.; Wang, Z.; Zhang, C. Gold-Coated Flower-Like TiO₂ Microparticles Wrapped with Reduced Graphene Oxide for SERS Monitoring and Photocatalytic Degradation of Organic Pollutants. *ACS Appl. Nano Mater.* **2022**, *5*, 15341–15352. [CrossRef]
16. Panneerselvam, R.; Liu, G.K.; Wang, Y.H.; Liu, J.Y.; Ding, S.Y.; Li, J.F.; Wu, D.Y.; Tian, Z.Q. Surface-Enhanced Raman Spectroscopy: Bottlenecks and Future Directions. *Chem. Commun.* **2017**, *54*, 10–25. [CrossRef]
17. Ling, X.; Xie, L.; Fang, Y.; Xu, H.; Zhang, H.; Kong, J.; Dresselhaus, M.S.; Zhang, J.; Liu, Z. Can Graphene Be Used as a Substrate for Raman Enhancement? *Nano Lett.* **2010**, *10*, 553–561. [CrossRef] [PubMed]
18. Lu, G.; Li, H.; Liusman, C.; Yin, Z.; Wu, S.; Zhang, H. Surface Enhanced Raman Scattering of Ag or Au Nanoparticle-Decorated Reduced Graphene Oxide for Detection of Aromatic Molecules. *Chem. Sci.* **2011**, *2*, 1817–1821. [CrossRef]
19. McPeak, K.M.; Jayanti, S.V.; Kress, S.J.P.; Meyer, S.; Iotti, S.; Rossinelli, A.; Norris, D.J. Plasmonic Films Can Easily Be Better: Rules and Recipes. *ACS Photonics* **2015**, *2*, 326–333. [CrossRef]
20. Ciuparu, D.; Ensuque, A.; Shafeev, G.; Bozon-Verduraz, F. Synthesis and apparent bandgap of nanophase zirconia. *J. Mater. Sci. Lett.* **2000**, *19*, 931–933. [CrossRef]
21. Pandiyan, R.; Vinothkumar, V.; Chen, T.W.; Chen, S.M.; Abinaya, M.; Rwei, S.P.; Hsu, H.Y.; Huang, C.W.; Yu, M.C. Synthesis of Ag@ZrO₂ Nanoparticles: A Sensitive Electrochemical Sensor for Determination of Antibiotic Drug Tinidazole. *Int. J. Electrochem. Sci.* **2022**, *17*, 220414. [CrossRef]
22. Ama, O.M.; Wilson, A.W.; Ray, S.S. Photoelectrochemical Degradation of Methylene Blue Dye under Visible Light Irradiation Using EG/Ag-ZrO₂ Nanocomposite Electrodes. *Int. J. Electrochem. Sci.* **2019**, *14*, 9982–10001. [CrossRef]
23. Shinde, H.M.; Kite, S.V.; Shirke, B.S.; Garadkar, K.M. Eco-Friendly Synthesis of Ag-ZrO₂ Nanocomposites for Degradation of Methylene Blue. *J. Mater. Sci. Mater. Electron.* **2021**, *32*, 14235–14247. [CrossRef]
24. Zhou, L.; Yang, J.; Wang, X.; Song, G.; Lu, F.; You, L.; Li, J. Ag Nanoparticles Decorated Ag@ZrO₂ Composite Nanospheres as Highly Active SERS Substrates for Quantitative Detection of Hexavalent Chromium in Waste Water. *J. Mol. Liq.* **2020**, *319*, 114158. [CrossRef]
25. Alyea, H.N.; Dutton, F.B. *Tested Demonstrations in Chemistry*, 6th ed.; Division of Chemical Education of the American Chemical Society: Easton, PA, USA, 1965.
26. Plasmonics.by. Available online: <http://plasmonics.by/en/> (accessed on 2 October 2023).
27. Basahel, S.N.; Ali, T.T.; Mokhtar, M.; Narasimharao, K. Influence of crystal structure of nanosized ZrO₂ on photocatalytic degradation of methyl orange. *Nanoscale Res. Lett.* **2015**, *10*, 73. [CrossRef] [PubMed]

28. Ciszak, C.; Mermoux, M.; Gutierrez, G.; Leprêtre, F.; Duriez, C.; Popa, I.; Fayette, L.; Chevalier, S. Raman spectra analysis of ZrO₂ thermally grown on Zircaloy substrates irradiated with heavy ion: Effects of oxygen isotopic substitution. *J. Raman. Spectrosc.* **2019**, *50*, 425–435. [[CrossRef](#)]
29. Li, C.; Li, M. UV Raman spectroscopic study on the phase transformation of ZrO₂, Y₂O₃–ZrO₂ and SO₄²⁻/ZrO₂. *J. Raman. Spectrosc.* **2002**, *33*, 301–308. [[CrossRef](#)]
30. Králik, B.; Chang, E.K.; Louie, S.G. Structural properties and quasiparticle band structure of zirconia. *Phys. Rev. B* **1998**, *57*, 7027. [[CrossRef](#)]
31. Emeline, A.; Kataeva, G.V.; Litke, A.S.; Rudakova, A.V.; Ryabchuk, V.K.; Serpone, N. Spectroscopic and Photoluminescence Studies of a Wide Band Gap Insulating Material: Powdered and Colloidal ZrO₂ Sols. *Langmuir* **1998**, *14*, 5011–5022. [[CrossRef](#)]
32. Alekperov, O.; Jahangirli, Z.; Paucar, R. First-principles lattice dynamics and Raman scattering in ionic conductor β-Ag₂S: Lattice dynamics and Raman scattering in ionic conductor β-Ag₂S. *Phys. Status Solidi B* **2016**, *253*, 2049–2055. [[CrossRef](#)]
33. Xiu, Z.; Zhang, Q.; Puppala, H.L.; Colvin, V.L.; Alvarez, P.J.J. Negligible Particle-Specific Antibacterial Activity of Silver Nanoparticles. *Nano Lett.* **2012**, *12*, 4271–4275. [[CrossRef](#)]
34. Greenwood, N.N.; Earnshaw, A. *Chemistry of the Elements*, 2nd ed.; Elsevier: Amsterdam, The Netherlands, 1997; ISBN 9780750633659.
35. Das, A.; Chakraborty, B.; Sood, A. Raman spectroscopy of graphene on different substrates and influence of defects. *Bull. Mater. Sci.* **2008**, *31*, 579–584. [[CrossRef](#)]
36. Calizo, I.; Balandin, A.A.; Bao, W.; Miao, F.; Lau, C.N. Temperature Dependence of the Raman Spectra of Graphene and Graphene Multilayers. *Nano Lett.* **2007**, *7*, 2645–2649. [[CrossRef](#)]
37. Lee, J.E.; Ahn, G.; Shim, J.; Lee, Y.S.; Ryu, S. Optical separation of mechanical strain from charge doping in graphene. *Nat. Commun.* **2012**, *3*, 1024. [[CrossRef](#)]
38. Ke, Q.; Wang, J. Graphene-based materials for supercapacitor electrodes—A review. *J. Mater.* **2016**, *2*, 37–54. [[CrossRef](#)]
39. Ferrari, A.; Basko, D. Raman spectroscopy as a versatile tool for studying the properties of graphene. *Nat. Nanotech.* **2013**, *8*, 235–246. [[CrossRef](#)] [[PubMed](#)]
40. Zhu, S.-E.; Yuan, S.; Janssen, G.C.A.M. Optical transmittance of multilayer graphene. *Europhys. Lett.* **2014**, *108*, 17007. [[CrossRef](#)]
41. Nair, R.R.; Blake, P.; Grigorenko, A.N.; Novoselov, K.S.; Booth, T.J.; Stauber, T.; Peres, N.M.; Geim, A.K. Fine Structure Constant Defines Visual Transparency of Graphene. *Science* **2008**, *320*, 1308. [[CrossRef](#)]
42. Watanabe, H.; Hayazawa, N.; Inouye, Y.; Kawata, S. DFT Vibrational Calculations of Rhodamine 6G Adsorbed on Silver: Analysis of Tip-Enhanced Raman Spectroscopy. *J. Phys. Chem. B* **2005**, *109*, 5012–5020. [[CrossRef](#)] [[PubMed](#)]
43. Hildebrandt, P.; Stockburger, M. Surface-Enhanced Resonance Raman Spectroscopy of Rhodamine 6G Adsorbed on Colloidal Silver. *J. Phys. Chem.* **1984**, *88*, 5935–5944. [[CrossRef](#)]
44. Rani, V.; Sharma, A.; Kumar, A.; Singh, P.; Thakur, S.; Singh, A.; Le, Q.V.; Nguyen, V.H.; Raizada, P. ZrO₂-Based Photocatalysts for Wastewater Treatment: From Novel Modification Strategies to Mechanistic Insights. *Catalysts* **2022**, *12*, 1418. [[CrossRef](#)]

Disclaimer/Publisher's Note: The statements, opinions and data contained in all publications are solely those of the individual author(s) and contributor(s) and not of MDPI and/or the editor(s). MDPI and/or the editor(s) disclaim responsibility for any injury to people or property resulting from any ideas, methods, instructions or products referred to in the content.